SLAC-PUB-15576

Gamma-ray Emission Concurrent with the Nova in the Symbiotic Binary V407 Cygni

The Fermi-LAT Collaboration*

submitted 19 May 2010; accepted 12 July 2010

Novae are thermonuclear explosions on a white dwarf surface fueled by mass accreted from a companion star. Current physical models posit that shocked expanding gas from the nova shell can produce X-ray emission but emission at higher energies has not been widely expected. Here, we report the *Fermi* Large Area Telescope detection of variable γ-ray (0.1–10 GeV) emission from the recently-detected optical nova of the symbiotic star V407 Cygni. We propose that the material of the nova shell interacts with the dense ambient medium of the red giant primary, and that particles can be accelerated effectively to produce π^0 decay γ-rays from proton-proton interactions. Emission involving inverse Compton scattering of the red giant radiation is also considered and is not ruled out.

V407 Cygni (V407 Cyg) is a binary system consisting of a Mira-type pulsating red giant (RG) with a white dwarf (WD) companion; these properties place it among the class of symbiotic binaries (*1*). Historically, although one of the more active symbiotic systems, V407 Cyg showed an optical spectrum in quiescence dominated by the Mira-like RG (M6 III) and

*All authors with their affiliations appear at the end of this paper.

Published in Science 329:817-821,2010 and arXiv:1008.3912.

KIPAC, SLAC National Accelerator Laboratory, 2575 Sand Hill Road, Menlo Park, CA 94025

Work supported in part by US Department of Energy under contract DE-AC02-76SF00515.

only weak emission lines, e.g., (*2*). Its infrared continuum (consistent with a dusty wind) and maser emission (*3*) are detected at levels similar to other symbiotic Miras [e.g., R Aqr (*4*)]. One outstanding anomaly of V407 Cyg is a strong Li I λ6707 line indicative of an overabundance of Li relative to normal Mira red giants (*5, 6*). Based on the 745-day pulsation period of the RG (*7*) and the Mira period-luminosity relation (*8*), we adopt the distance, $D = 2.7$ kpc, estimated as the mean derived from photometry in three near-infrared bands assuming an extinction, $E_{\rm B-V} = 0.57$ (*2*).

A nova outburst from V407 Cyg was detected on 10 March 2010 (*9*); it had a magnitude approximately 6.9 in an unfiltered CCD image obtained at 19:08 UT. Subsequent densely sampled observations show the outburst was followed by a smooth decay, though the precise epoch of the nova is formally uncertain by up to 3 days due to the time gap from the pre-outburst image (Fig. 1). Monitoring of the source over the past two years indicates pre-outburst magnitude values in the range 9–12 [see the supporting online material (SOM)]. V407 Cyg has been monitored optically for decades and has shown earlier signs of optical brightening on month-timescales by 1–2 magnitudes in the B and V bands (around 1936 and 1998) from typical V band magnitudes of 13–16 (*2,10,11*), but the magnitude of the recent nova was unprecedented.

Here we report on a high-energy γ-ray source (Fig. 2) positionally coincident with V407 Cyg detected after the nova (*12*) during routine automated processing of all-sky monitoring data from the *Fermi* Large Area Telescope (LAT) (*13*). A γ-ray light curve (one-day time bins) of this source generated from an analysis of all LAT data reveals that the first significant detection (4.3σ) was in fact on 10 March indicating the γ-ray activity began on the same day as the reported optical maximum of V407 Cyg (Fig. 1, SOM). The observed 10 March flux is up to a factor of 3 larger than the one-day upper limits (unless otherwise noted, 95$\%$ confidence limits are reported throughout) on the pre-outburst days. To further isolate the onset of detectable γ-ray emission, we divided the 10 March data into 6-hour intervals and the first indication of

a signal was a marginal detection in the 12h–18h bin (2.8σ). This was followed by a highly significant detection (at 5.7σ) in the last 6-hr bin (18h–24h) which had a peak flux that was a factor of $\gtrsim 3$ larger than that of the marginal detection and the limits from earlier in the day (SOM). The initial detection of the γ-ray source by the *Fermi*-LAT in the latter 1/2-day of 10 March is consistent with the time of the optical nova discovery.

The peak flux in γ-rays (defined on one-day segments) was observed between 13–14 March, 3–4 days after the initial γ-ray detection, and with a factor of 2 greater flux (9×10^{-7} photons cm^{-2} s^{-1}). Analyzing data up to mid-April, the last day with a significant detection ($>3\sigma$) of the variable γ-ray source is 25 March, amounting to a total lifetime of activity of two weeks. Defining an 'active' period (*14*) from 10 March 18:00 to 29 March 00:00, we obtained a γ-ray position (Fig. 2) from the cumulative exposure that is 0.040° offset from the optical position of V407 Cyg, which is within the LAT 95% confidence circle (radius = 0.062°). The average spectral energy distribution (SED) of the *Fermi*-LAT γ-ray source during the defined active period can be described with an exponentially cut off power-law model (SOM) with a flux (>100 MeV) of $(4.4 \pm 0.4) \times 10^{-7}$ photons cm^{-2} s^{-1} (overall source significance of 18.1σ). A likelihood ratio test demonstrates that the addition of the exponential cut off improves the fit at the 4.9σ level compared to a simpler single power-law model. We find no evidence for spectral variability over the duration of the active γ-ray period (SOM). Analyzing data from the two weeks (29 March to 12 April) following the active period collectively gives a significance of only 1.6σ (flux upper limit of 0.8×10^{-7} photons cm^{-2} s^{-1}), indicating that the flux has declined below detectability. Overall, the γ-ray source is brightest at earlier times, consistent with the optical behavior of V407 Cyg. The coincident localization and the observed correlated variability imply that the optical nova is the source of the variable γ-ray flux.

Nuclear γ-ray lines and continuum emission from novae at $\lesssim 1$ MeV energies have been considered (*15*), but the *Fermi*-LAT detection of V407 Cyg shows unequivocally that novae can

generate high-energy (>100 MeV) γ-rays. The >100 MeV γ-ray luminosity, its spectrum, and light curve can be understood broadly as consequences of shock acceleration taking place in a nova shell. Such a nova shell is produced by thermonuclear energy release on the WD and initially expands freely into a very dense medium consisting of the RG wind and atmosphere present in the binary system prior to the nova. The radio source detected from V407 Cyg over 22–28 March (*16,17*), and subsequent imaging which revealed the emission to be predominantly extended at few milli-arcsecond resolution (*18*), is consistent with a picture of an extended shell as was found in the 2006 RS Oph nova outburst (*19, 20*).

An initially spherical shell can sweep up mass from the companion RG wind asymmetrically and will reach a deceleration phase during which it expands adiabatically (*21*) with different temporal behavior in different directions from the WD center. Fermi acceleration of protons and electrons takes place in the outgoing nova shock during both the free expansion phase and deceleration phase, and we show that the measured γ-ray spectrum can be explained by π^0 decay γ-rays from proton-proton (pp) collisions or inverse Compton (IC) scattering of infrared photons from the RG by electrons. In both these scenarios, the γ-ray light curve in conjunction with the delayed rise of the X-ray flux can be explained qualitatively as a geometrical effect of the nova shell evolution.

The measured optical peak magnitude ≈ 7 of V407 Cyg (*9*) over one day, implies an energy release of $\geq 3 \times 10^{42}$ ergs at visible frequencies (after extinction correction). The kinetic energy of the ejecta in the nova shell, $\mathcal{E}_{\rm k} \sim 10^{44}$ ergs, can be estimated assuming a nova shell mass, $M_{\rm ej} \sim 10^{-6}\, M_\odot$ [which is a plausible value for a massive WD, $>1.25 M_\odot$ (*22, 23*)], and the velocity, $v_{\rm ej} = 3200 \pm 345$ km s^{-1}, inferred from an Hα line width measurement on 14 March (SOM). The velocity of the outgoing shock wave is initially $v_{\rm sh} \sim v_{\rm ej}$. The onset of the deceleration phase and subsequent evolution of the shock wave are determined by the density of the RG stellar wind and atmosphere surrounding the nova shell, which depends on two poorly

constrained parameters – the WD-RG separation (a) and the RG mass loss rate in the wind ($\dot{M}_{\rm w}$). As we will discuss shortly, the detection of the γ-ray flux within one day of the optical detection of the nova, a peak duration of 3-4 days, and subsequent decay within 15 days after the optical nova can be modeled as emission from the nova shell in a dense environment and mostly from along the WD-RG axis assuming an inverse-square law wind density profile from the RG center, with $a \sim 10^{14}$ cm, and $\dot{M}_{\rm w} \sim 3 \times 10^{-7}\,M_\odot$ yr^{-1}. Both these values are a factor ≈ 2 smaller than those suggested previously for the V407 Cyg system (*2*).

The density of particles in the RG wind is $n(R) = \dot{M}_{\rm w}\,[4\pi\,(R^2 + a^2 - 2aR\cos\theta)\,v_{\rm w}\,\bar{m}]^{-1}$. Here, the RG wind velocity, $v_{\rm w} \approx 10$ km s^{-1}, is based on optical spectra (SOM), the mean particle mass is $\bar{m} \approx 10^{-24}$ g, R is the distance from the WD center, and θ is the polar angle relative to the WD center. The energy density in the RG radiation field is similarly, $u_{\rm IR}(R) = L_{\rm IR}\,[4\pi(R^2 + a^2 - 2aR\cos\theta)\,c]^{-1}$. The RG luminosity, $L_{\rm IR} \approx 10^4 L_\odot$ (*2,11*), is consistent with a spectral fit to post-nova infrared measurements with a temperature of ≈ 2500 K (SOM). Near the WD surface ($R \approx 0.01\ R_\odot$), these densities are $n \sim 10^8$ cm^{-3} and $u_{\rm IR} \sim 0.01$ erg cm^{-3}, and increase by up to an order of magnitude when the nova shell approaches the RG surface (i.e., along $\theta \approx 0^\circ$) at a radius $r_{\rm RG} \approx 500\ R_\odot$. An equipartition of the energy density in the magnetic field expected to arise from turbulent motions in the wind, to the thermal energy density in the RG wind with temperature $T_{\rm w} \approx 700$ K (*2*) gives a mean magnetic field, $B_{\rm sh}(R) = [32\pi\,n(R)\,k\,T_{\rm w}]^{1/2} \sim 0.03$ G in the shock wave when it is near the WD. Electrons and protons can be accelerated efficiently in this magnetic field (*24*) and interact with the surrounding RG wind particles and radiation.

The time scale for pp interactions for a π^0 model to produce γ-rays in the shock wave is $t_{\rm pp} \approx 1/[4\,n(R)\,c\,\sigma_{\rm pp}] \sim 2.8 \times 10^6$ s when the nova shell is near the WD. Here, $\sigma_{\rm pp} \approx 3 \times 10^{-26}$ cm^2 is the pp cross-section. Thus, $t/t_{\rm pp} \sim 3\%$ of the protons can interact to produce π^0 emission on a time scale, $t = 1$ day. In an IC scenario, the cooling time scale

for electrons with energy $E_{\rm e} \approx 5$ GeV that up-scatter 2500 K photons to ≈ 100 MeV is $t_{\rm IC} \approx (3/4)\, m_{\rm e}^2\, c^3\, [\sigma_{\rm T}\, E_{\rm e}\, u_{\rm IR}(R)]^{-1} \sim 3.1 \times 10^5$ s. Thus, $t/t_{\rm IC} \sim 28\%$ of the electrons produce γ-rays efficiently in a time scale, $t = 1$ day. The efficiency for γ-ray production in both the π^0 and IC models increases substantially in the part of the nova shell that expands towards the RG ($\theta \sim 0^\circ$) and reaches the deceleration phase, by accumulating RG wind and atmospheric material of mass equal to $M_{\rm ej}$, at a distance $\sim 7 \times 10^{13}$ cm in about 2.5 days. The efficiency decreases rapidly in the part of the shell that expands away from the RG ($\theta \geq 90^\circ$) because of a decreasing density in both the RG wind and radiation.

In our scenario, most of the γ-rays come from the part of the nova shell approaching the RG. This can qualitatively explain the basic features of the γ-ray light curve (Fig. 1): (i) its onset within days of the optical nova and the peak flux reached in three days due to an increasing efficiency for pp interactions and an increasing volume of the shock-accelerated particles, and (ii) the decline in the flux after about five days due to weakening of the shock wave after reaching the deceleration phase. A highly significant one-day detection (6.5σ) of an increase in γ-ray flux 9 days after the nova discovery (Fig. 1) could be due to the nova shell hitting a part of the RG surface or a nearby remnant of high density with a size scale of $\sim 10^{13}\, (v_{\rm sh}/1500\, {\rm km\ s^{-1}})\, (t/1\, {\rm day})$ cm.

A representative π^0 decay model is shown in Fig. 3 fitting the LAT data with a cosmic-ray proton spectrum in the form of an exponentially cut off power-law, $N_{\rm p} = N_{\rm p,0}\, (W_{\rm p} + m_{\rm p}\, c^2)^{-s_{\rm p}}\, e^{-W_{\rm p}/E_{\rm cp}}$, where $E_{\rm cp}$, $W_{\rm p}$, and $m_{\rm p}$ are the cutoff energy, kinetic energy, and mass of the proton, respectively. The γ-ray spectrum is well reproduced with a spectral index, $s_{\rm p} = 2.15^{+0.45}_{-0.28}$, similar to the expected spectrum from the Fermi acceleration mechanism, with $E_{\rm cp} = 32^{+85}_{-8}$ GeV (1σ uncertainties) (SOM). The total energy in γ-rays above 100 MeV integrated over the active period is $\mathcal{E}_\gamma \approx 3.6 \times 10^{41}$ erg. The total energy in protons is $\mathcal{E}_{\rm p} \approx \epsilon_{\rm p}^{-1} \langle E_{\rm p}/E_\gamma \rangle \mathcal{E}_\gamma$, where $\epsilon_{\rm p}$ is the mean efficiency for pp interactions and $1/\langle E_{\rm p}/E_\gamma \rangle \approx 0.2$ is the mean fraction

of proton energy transfer to γ-rays per interaction in the $E_\gamma \geq 100$ MeV range. The ratio of the total energy in protons that produce γ-rays to the kinetic energy, $\mathcal{E}_{\rm p}/\mathcal{E}_{\rm k} \sim 9\%$, with $\epsilon_{\rm p} \sim 0.2$ averaged over the γ-ray source lifetime of 15 days and the whole nova shell, similar to 1–10% estimated in supernova remnants (*25*). The ratio, however, is larger when considering dominant γ-ray emission coming mostly from the part of the shell that expands towards the RG.

The leptonic model is represented in Fig. 3 as the total of the IC spectrum plus a small contribution from bremsstrahlung emission, that arises from scattering of electrons with protons of density $n(R)$ in the shock wave (SOM). The exponentially cut off power-law electron spectrum, $N_{\rm e} = N_{\rm e,0}\, W_{\rm e}^{-s_{\rm e}}\, e^{-W_{\rm e}/E_{\rm ce}}$, where $E_{\rm ce}$ and $W_{\rm e}$ are the cutoff energy and kinetic energy of electrons (GeV), respectively, reproduces the γ-ray spectrum with $s_{\rm e} = -1.75^{+2.40}_{-0.59}$ and $E_{\rm ce} = 3.2^{+2.6}_{-0.1}$ GeV (1σ uncertainties) (SOM). The total number of electrons required in steady state is $N_{\rm e,0} \approx 4 \times 10^{42}$, with a mean energy of 8.7 GeV which is larger than $E_{\rm ce}$ because of the steep spectrum. The total energy in electrons over 15 days of γ-ray emission is $\mathcal{E}_{\rm e} \approx 4 \times 10^{41}$ ergs, averaged over the nova shell. Thus the total energy in electrons that produce γ-rays in the IC model is a small fraction of the kinetic energy in the shell ($\mathcal{E}_{\rm e}/\mathcal{E}_{\rm k} \sim 0.4\%$).

X-ray emission detected from V407 Cyg with the *Swift* X-ray Telescope (XRT) as early as three days after the onset of the optical nova (Fig. 1) is likely due to shock-heating of ambient gas (*26,27*). The X-ray flux starts rising significantly about two weeks after the nova, coinciding with when the γ-ray flux declines below detectability. In our geometric scenario, the sharply rising X-ray flux is due to the increasing volume of shocked gas in the nova shell expanding in the direction away from the RG. The X-ray flux peaks about 30 days after the explosion, and its subsequent slow decline is consistent with the longer time scale of the deceleration phase.

The *Fermi*-LAT detection of V407 Cyg was a surprise, and adds novae as a source class to the high-energy γ-ray sky. The particle acceleration mechanism and the γ-ray emission scenarios outlined here require the mass donor to be a red giant, i.e., a nova in a symbiotic

system. Interestingly, several symbiotic stars are known to be recurrent novae (i.e., systems observed to have undergone multiple thermonuclear runaways within the last century), and recurrent novae are often considered candidate progenitors of Type Ia supernovae (*28*). V407 Cyg may also belong to this class of binaries, and we have adopted parameters that are consistent with such a classification in modeling the γ-ray emission. These sources can in general have dramatic influence on the local interstellar medium and Galactic cosmic rays but few binary systems with a WD are known to have a similar environment, hence we expect γ-ray novae to be rare.

References and Notes

1. S. J. Kenyon, in Evolutionary Processes in Interacting Binary Stars, Edited by Y. Kondo *et al.*, IAU Symp. 151, 137 (1992).

2. U. Munari, R. Margoni, R. Stagni, *Mon. Not. R. Astron. Soc.* **242**, 653 (1990).

3. S. Deguchi, J.-I. Nakashima, T. Miyata, Y. Ita, *Publ. Astron. Soc. Japan* **57**, 933 (2005).

4. R. J. Ivison, E. R. Seaquist, P. J. Hall, *Mon. Not. R. Astron. Soc.* **269**, 218 (1994).

5. S. Y. Shugarov, A. A. Tatarnikova, E. A. Kolotilov, V. I. Shenavrin, B. F. Yudin, *Baltic Astronomy*, **16**, 23 (2007).

6. A. A. Tatarnikova *et al.*, *Mon. Not. R. Astron. Soc.* **344** 1233 (2003).

7. L. Meinunger, Mitt. Veranderl. Sterne. **87**, 111 (1966).

8. I. S. Glass, M. W. Feast, *Mon. Not. R. Astron. Soc.* **199**, 245 (1982).

9. K. Nishiyama, F. Kabashima, IAU Central Bureau for Astronomical Telegrams, reported by H. Maehara, No. 2199 (2010).

10. C. Hoffmeister, Veröff. Sternw. Sonneberg. **1**, 295 (1949).

11. E. A. Kolotilov, V. I. Shenavrin, S. Y. Shugarov, B. F. Yudin, *Astron. Rep.* **47**, 777 (2003).

12. C. C. Cheung *et al.* (*Fermi*-LAT collaboration), *The Astronomer's Telegram* **2487**, 1 (2010).

13. W. B. Atwood *et al.* (*Fermi*-LAT collaboration), *Astrophys. J.* **697**, 1071 (2009).

14. The window was extended by three days to include any late low-level emission which would not be detectable on any individual daily bin.

15. M. Hernanz, in Classical Novae, 2nd ed., Edited by M. F. Bode & A. Evans, Cambridge University Press (2008), p. 252.

16. I. Nestoras *et al.*, *The Astronomer's Telegram* **2506**, 1 (2010).

17. G. C. Bower, R. Forster, C. C. Cheung, *The Astronomer's Telegram* **2529**, 1 (2010).

18. M. Giroletti *et al.*, *The Astronomer's Telegram* **2536**, 1 (2010).

19. T. J. O'Brien *et al.*, *Nature* **442**, 279 (2006).

20. M. P. Rupen, A. J. Mioduszewski, J. L. Sokoloski, *Astrophys. J.* **688**, 559 (2008).

21. L. I. Sedov, Similarity and Dimensional Methods in Mechanics, New York: Academic Press (1959).

22. S. Starrfield, W. M. Sparks, J. W. Truran, M. C. Wiescher, *Astrophys. J. Supp.* **127**, 485 (2000).

23. O. Yaron, D. Prialnik, M. M. Shara, A. Kovetz, *Astrophys. J.* **623**, 398 (2005).

24. V. Tatischeff, M. Hernanz, *Astrophys. J. Lett.* **663**, L101 (2007).

25. A. A. Abdo *et al.* (*Fermi*-LAT collaboration), *Astrophys. J. Lett.* **710**, L92 (2010).

26. J. L. Sokoloski, G. J. M. Luna, K. Mukai, S. J. Kenyon, *Nature* **442**, 276 (2006).

27. J. J. Drake *et al. Astrophys. J.* **691**, 418 (2009).

28. W. M. Wood-Vasey, J. L. Sokoloski, *Astrophys. J. Lett.* **645**, 53 (2006).

29. A. A. Abdo *et al.* (*Fermi*-LAT collaboration), *Astrophys. J. Supp.* **188**, 405 (2010).

30. The *Fermi* LAT Collaboration acknowledges support from a number of agencies and institutes for both development and the operation of the LAT as well as scientific data analysis. These include NASA and DOE in the United States, CEA/Irfu and IN2P3/CNRS in France, ASI and INFN in Italy, MEXT, KEK, and JAXA in Japan, and the K. A. Wallenberg Foundation, the Swedish Research Council and the National Space Board in Sweden. Additional support from INAF in Italy and CNES in France for science analysis during the operations phase is also gratefully acknowledged. P. K. acknowledges support from AI ASCR (Ondrejov) in the Czech Republic. We acknowledge with thanks the variable star observations from the AAVSO International Database contributed by observers worldwide and used in this research.

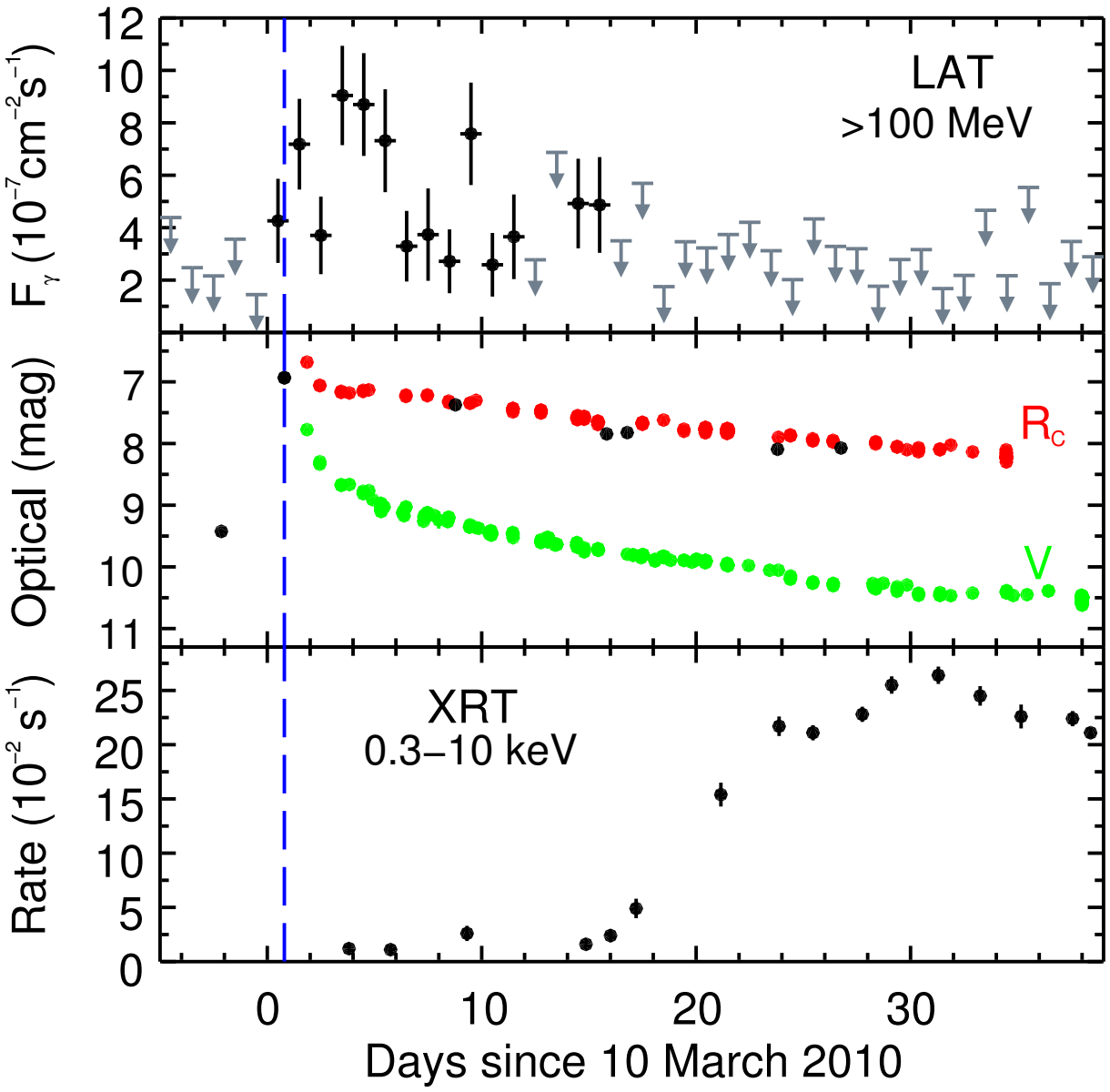

Fig. 1. Light curves of V407 Cyg in γ-rays from the *Fermi*-LAT (top), optical (middle), and X-rays from *Swift* (bottom). Vertical bars indicate 1σ statistics errors for all data (the errors are smaller than the points in the optical). For the γ-ray data, gray arrows indicate 2σ upper limits, and horizontal bars indicate the one-day binning. In the optical, unfiltered (black), $R_{\rm C}$ (red), and V (green) band magnitudes are shown (SOM). The vertical dashed blue line indicates the epoch of the optical nova detection; the γ-ray peak occurred 3–4 days later.

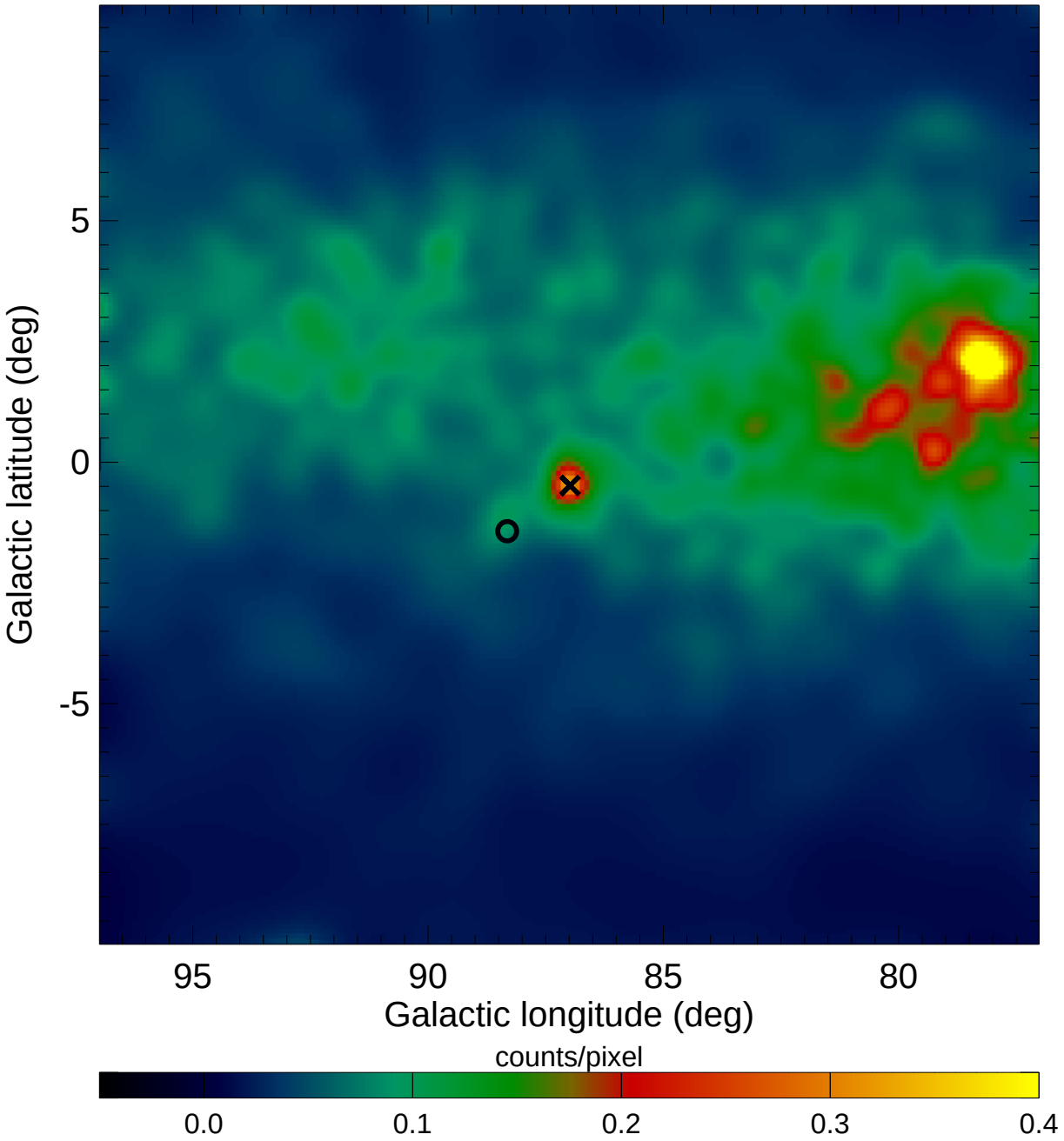

Fig. 2. *Fermi*-LAT γ-ray counts (200 MeV–100 GeV) map from 10 March 18:00 – 29 March 00:00 2010 in the region around the position of the γ-ray nova source V407 Cyg (marked by black cross) at $l = 86.958°$, $b = -0.513°$ (R. A. = 315.551°, Dec. = +45.737°, J2000.0). The map was adaptively smoothed by imposing a minimum signal-to-noise ratio of 7. The closest known γ-ray source is contained in the 1st year LAT catalog (1FGL J2111.3+4607; marked by the black circle) (*29*), $\sim$1.5° away from the star's optical position. The bright source at ($l = 78.2°$, $b = +2.1°$) is LAT PSR J2021+4026.

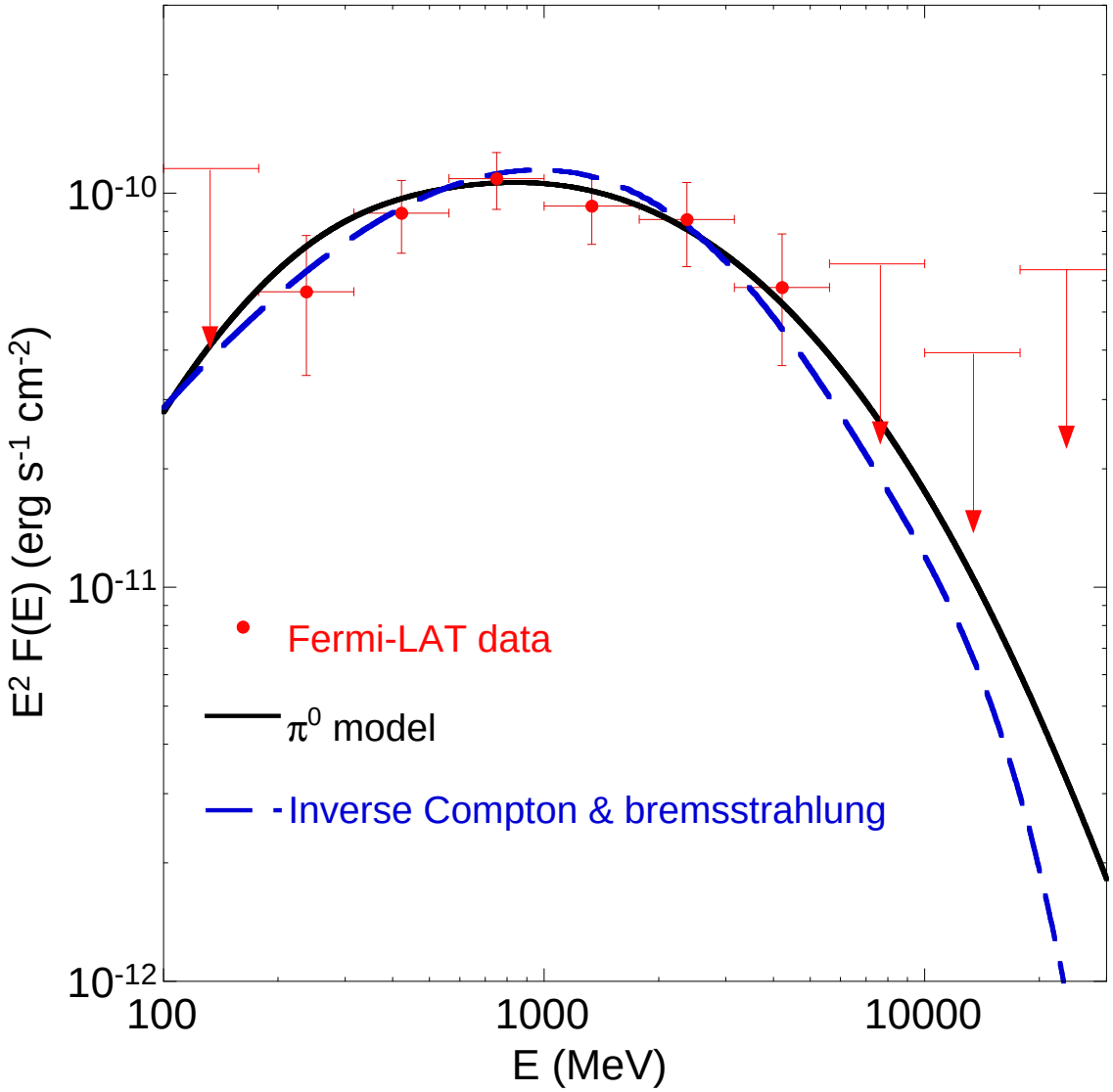

Fig. 3. SED of V407 Cyg in MeV/GeV γ-rays measured by the *Fermi*-LAT over the period 10 March 18:00 – 29 March 00:00 2010. Vertical bars indicate 1σ statistical errors, arrows indicate 2σ upper limits, and horizontal bars indicate energy ranges. The best-fit π^0 (black solid line) and leptonic (blue dashed line) models are indicated.

The Fermi-LAT Collaboration

A. A. Abdo[1,2], M. Ackermann[3], M. Ajello[3], W. B. Atwood[4], L. Baldini[5], J. Ballet[6], G. Barbiellini[7,8], D. Bastieri[9,10], K. Bechtol[3], R. Bellazzini[5], B. Berenji[3], R. D. Blandford[3], E. D. Bloom[3], E. Bonamente[11,12], A. W. Borgland[3], A. Bouvier[3], T. J. Brandt[13,14], J. Bregeon[5], A. Brez[5], M. Brigida[15,16], P. Bruel[17], R. Buehler[3], T. H. Burnett[18], S. Buson[9,10], G. A. Caliandro[19], R. A. Cameron[3], P. A. Caraveo[20], S. Carrigan[10], J. M. Casandjian[6], C. Cecchi[11,12], Ö. Çelik[21,22,23], E. Charles[3], S. Chaty[6], A. Chekhtman[1,24], C. C. Cheung[1,2*], J. Chiang[3], S. Ciprini[12], R. Claus[3], J. Cohen-Tanugi[25], J. Conrad[26,27,28], S. Corbel[6,29], R. Corbet[21,23], M. E. DeCesar[21,30], P. R. den Hartog[3], C. D. Dermer[1], F. de Palma[15,16], S. W. Digel[3], D. Donato[22,30], E. do Couto e Silva[3], P. S. Drell[3], R. Dubois[3], G. Dubus[31,32], D. Dumora[33,34], C. Favuzzi[15,16], S. J. Fegan[17], E. C. Ferrara[21], P. Fortin[17], M. Frailis[35,36], L. Fuhrmann[37], Y. Fukazawa[38], S. Funk[3], P. Fusco[15,16], F. Gargano[16], D. Gasparrini[39], N. Gehrels[21], S. Germani[11,12], N. Giglietto[15,16], F. Giordano[15,16], M. Giroletti[40], T. Glanzman[3], G. Godfrey[3], I. A. Grenier[6], M.-H. Grondin[33,34], J. E. Grove[1], S. Guiriec[41], D. Hadasch[42], A. K. Harding[21], M. Hayashida[3], E. Hays[21], S. E. Healey[3], A. B. Hill[31,32*], D. Horan[17], R. E. Hughes[14], R. Itoh[38], P. Jean[13*], G. Jóhannesson[3], A. S. Johnson[3], R. P. Johnson[4], T. J. Johnson[21,30], W. N. Johnson[1], T. Kamae[3], H. Katagiri[38], J. Kataoka[43], M. Kerr[18], J. Knödlseder[13], E. Koerding[6], M. Kuss[5], J. Lande[3], L. Latronico[5], S.-H. Lee[3], M. Lemoine-Goumard[33,34], M. Llena Garde[26,27], F. Longo[7,8], F. Loparco[15,16], B. Lott[33,34], M. N. Lovellette[1], P. Lubrano[11,12], A. Makeev[1,24], M. N. Mazziotta[16], W. McConville[21,30], J. E. McEnery[21,30], J. Mehault[25], P. F. Michelson[3], T. Mizuno[38], A. A. Moiseev[22,30], C. Monte[15,16], M. E. Monzani[3], A. Morselli[44], I. V. Moskalenko[3], S. Murgia[3], T. Nakamori[43], M. Naumann-Godo[6], I. Nestoras[37], P. L. Nolan[3], J. P. Norris[45], E. Nuss[25], M. Ohno[46], T. Ohsugi[47], A. Okumura[46], N. Omodei[3], E. Orlando[48], J. F. Ormes[45], M. Ozaki[46], D. Paneque[3], J. H. Panetta[3], D. Parent[1,24], V. Pelassa[25], M. Pepe[11,12], M. Pesce-Rollins[5], F. Piron[25], T. A. Porter[3], S. Rainò[15,16], R. Rando[9,10], P. S. Ray[1], M. Razzano[5], S. Razzaque[1,2*], N. Rea[19], A. Reimer[49,3], O. Reimer[49,3], T. Reposeur[33,34], J. Ripken[26,27], S. Ritz[4], R. W. Romani[3],

M. Roth[18], H. F.-W. Sadrozinski[4], A. Sander[14], P. M. Saz Parkinson[4], J. D. Scargle[50], F. K. Schinzel[37], C. Sgrò[5], M. S. Shaw[3], E. J. Siskind[51], D. A. Smith[33,34], P. D. Smith[14], K. V. Sokolovsky[37,52], G. Spandre[5], P. Spinelli[15,16], Ł. Stawarz[46,53], M. S. Strickman[1], D. J. Suson[54], H. Takahashi[47], T. Takahashi[46], T. Tanaka[3], Y. Tanaka[46], J. B. Thayer[3], J. G. Thayer[3], D. J. Thompson[21], L. Tibaldo[9,10,6,55], D. F. Torres[19,42], G. Tosti[11,12], A. Tramacere[3,56,57], Y. Uchiyama[3], T. L. Usher[3], J. Vandenbroucke[3], V. Vasileiou[22,23], N. Vilchez[13], V. Vitale[44,58], A. P. Waite[3], E. Wallace[18], P. Wang[3], B. L. Winer[14], M. T. Wolff[1], K. S. Wood[1*], Z. Yang[26,27], T. Ylinen[59,60,27], M. Ziegler[4], H. Maehara[61], K. Nishiyama[62], F. Kabashima[62], U. Bach[37], G. C. Bower[63], A. Falcone[64], J. R. Forster[63,65], A. Henden[66], K. S. Kawabata[47], P. Koubsky[67], K. Mukai[21,23], T. Nelson[21,23], S. R. Oates[68], K. Sakimoto[38], M. Sasada[38], V. I. Shenavrin[69], S. N. Shore[5,70], G. K. Skinner[22,30], J. Sokoloski[71], M. Stroh[62], A. M. Tatarnikov[69], M. Uemura[47], G. M. Wahlgren[72,21], M. Yamanaka[38]

1. Space Science Division, Naval Research Laboratory, Washington, DC 20375, USA

2. National Research Council Research Associate, National Academy of Sciences, Washington, DC 20001, USA

3. W. W. Hansen Experimental Physics Laboratory, Kavli Institute for Particle Astrophysics and Cosmology, Department of Physics and SLAC National Accelerator Laboratory, Stanford University, Stanford, CA 94305, USA

4. Santa Cruz Institute for Particle Physics, Department of Physics and Department of Astronomy and Astrophysics, University of California at Santa Cruz, Santa Cruz, CA 95064, USA

5. Istituto Nazionale di Fisica Nucleare, Sezione di Pisa, I-56127 Pisa, Italy

6. Laboratoire AIM, CEA-IRFU/CNRS/Université Paris Diderot, Service d'Astrophysique, CEA Saclay, 91191 Gif sur Yvette, France

7. Istituto Nazionale di Fisica Nucleare, Sezione di Trieste, I-34127 Trieste, Italy
8. Dipartimento di Fisica, Università di Trieste, I-34127 Trieste, Italy
9. Istituto Nazionale di Fisica Nucleare, Sezione di Padova, I-35131 Padova, Italy
10. Dipartimento di Fisica “G. Galilei”, Università di Padova, I-35131 Padova, Italy
11. Istituto Nazionale di Fisica Nucleare, Sezione di Perugia, I-06123 Perugia, Italy
12. Dipartimento di Fisica, Università degli Studi di Perugia, I-06123 Perugia, Italy
13. Centre d’Étude Spatiale des Rayonnements, CNRS/UPS, BP 44346, F-30128 Toulouse Cedex 4, France
14. Department of Physics, Center for Cosmology and Astro-Particle Physics, The Ohio State University, Columbus, OH 43210, USA
15. Dipartimento di Fisica “M. Merlin” dell’Università e del Politecnico di Bari, I-70126 Bari, Italy
16. Istituto Nazionale di Fisica Nucleare, Sezione di Bari, 70126 Bari, Italy
17. Laboratoire Leprince-Ringuet, École polytechnique, CNRS/IN2P3, Palaiseau, France
18. Department of Physics, University of Washington, Seattle, WA 98195-1560, USA
19. Institut de Ciencies de l’Espai (IEEC-CSIC), Campus UAB, 08193 Barcelona, Spain
20. INAF-Istituto di Astrofisica Spaziale e Fisica Cosmica, I-20133 Milano, Italy
21. NASA Goddard Space Flight Center, Greenbelt, MD 20771, USA

22. Center for Research and Exploration in Space Science and Technology (CRESST) and NASA Goddard Space Flight Center, Greenbelt, MD 20771, USA

23. Department of Physics and Center for Space Sciences and Technology, University of Maryland Baltimore County, Baltimore, MD 21250, USA

24. George Mason University, Fairfax, VA 22030, USA

25. Laboratoire de Physique Théorique et Astroparticules, Université Montpellier 2, CNRS/IN2P3, Montpellier, France

26. Department of Physics, Stockholm University, AlbaNova, SE-106 91 Stockholm, Sweden

27. The Oskar Klein Centre for Cosmoparticle Physics, AlbaNova, SE-106 91 Stockholm, Sweden

28. Royal Swedish Academy of Sciences Research Fellow, funded by a grant from the K. A. Wallenberg Foundation

29. Institut universitaire de France, 75005 Paris, France

30. Department of Physics and Department of Astronomy, University of Maryland, College Park, MD 20742, USA

31. Université Joseph Fourier - Grenoble 1 / CNRS, laboratoire d'Astrophysique de Grenoble (LAOG) UMR 5571, BP 53, 38041 Grenoble Cedex 09, France

32. Funded by contract ERC-StG-200911 from the European Community

33. CNRS/IN2P3, Centre d'Études Nucléaires Bordeaux Gradignan, UMR 5797, Gradignan, 33175, France

34. Université de Bordeaux, Centre d'Études Nucléaires Bordeaux Gradignan, UMR 5797, Gradignan, 33175, France

35. Dipartimento di Fisica, Università di Udine and Istituto Nazionale di Fisica Nucleare, Sezione di Trieste, Gruppo Collegato di Udine, I-33100 Udine, Italy

36. Osservatorio Astronomico di Trieste, Istituto Nazionale di Astrofisica, I-34143 Trieste, Italy

37. Max-Planck-Institut für Radioastronomie, Auf dem Hügel 69, 53121 Bonn, Germany

38. Department of Physical Sciences, Hiroshima University, Higashi-Hiroshima, Hiroshima 739-8526, Japan

39. Agenzia Spaziale Italiana (ASI) Science Data Center, I-00044 Frascati (Roma), Italy

40. INAF Istituto di Radioastronomia, 40129 Bologna, Italy

41. Center for Space Plasma and Aeronomic Research (CSPAR), University of Alabama in Huntsville, Huntsville, AL 35899, USA

42. Institució Catalana de Recerca i Estudis Avançats (ICREA), Barcelona, Spain

43. Research Institute for Science and Engineering, Waseda University, 3-4-1, Okubo, Shinjuku, Tokyo, 169-8555 Japan

44. Istituto Nazionale di Fisica Nucleare, Sezione di Roma "Tor Vergata", I-00133 Roma, Italy

45. Department of Physics and Astronomy, University of Denver, Denver, CO 80208, USA

46. Institute of Space and Astronautical Science, JAXA, 3-1-1 Yoshinodai, Sagamihara, Kanagawa 229-8510, Japan

47. Hiroshima Astrophysical Science Center, Hiroshima University, Higashi-Hiroshima, Hiroshima 739-8526, Japan

48. Max-Planck Institut für extraterrestrische Physik, 85748 Garching, Germany

49. Institut für Astro- und Teilchenphysik and Institut für Theoretische Physik, Leopold-Franzens-Universität Innsbruck, A-6020 Innsbruck, Austria

50. Space Sciences Division, NASA Ames Research Center, Moffett Field, CA 94035-1000, USA

51. NYCB Real-Time Computing Inc., Lattingtown, NY 11560-1025, USA

52. Astro Space Center of the Lebedev Physical Institute, 117810 Moscow, Russia

53. Astronomical Observatory, Jagiellonian University, 30-244 Kraków, Poland

54. Department of Chemistry and Physics, Purdue University Calumet, Hammond, IN 46323-2094, USA

55. Partially supported by the International Doctorate on Astroparticle Physics (IDAPP) program

56. Consorzio Interuniversitario per la Fisica Spaziale (CIFS), I-10133 Torino, Italy

57. INTEGRAL Science Data Centre, CH-1290 Versoix, Switzerland

58. Dipartimento di Fisica, Università di Roma “Tor Vergata”, I-00133 Roma, Italy

59. Department of Physics, Royal Institute of Technology (KTH), AlbaNova, SE-106 91 Stockholm, Sweden

60. School of Pure and Applied Natural Sciences, University of Kalmar, SE-391 82 Kalmar, Sweden

61. Kwasan and Hida Observatories, Kyoto University, Kyoto 607-8471, Japan

62. Miyaki-Argenteus Observatory, Miyaki-cho, Saga-ken, Japan

63. Department of Astronomy, University of California, Berkeley, CA 94720-3411, USA

64. Department of Astronomy and Astrophysics, Pennsylvania State University, University Park, PA 16802, USA

65. Hat Creek Observatory, Hat Creek, CA 96040, USA

66. American Association of Variable Star Observers, Cambridge, MA 02138, USA

67. Astronomical Institute, Academy of Sciences of the Czech Republic, Ondřejov, Czech Republic

68. Mullard Space Science Laboratory, University College London, Holmbury St. Mary, Dorking, Surrey, RH5 6NT, UK

69. Sternberg Astronomical Institute, Moscow University, Moscow, Russia

70. Dipartimento di Fisica ”Enrico Fermi” , Università di Pisa, Pisa I-56127, Italy

71. Columbia Astrophysics Laboratory, Columbia University, New York, NY 10027, USA

72. Catholic University of America, Washington, DC 20064, USA

* To whom correspondence should be addressed.

E-mail: Teddy.Cheung.ctr@nrl.navy.mil (C.C.C.); Adam.Hill@obs.ujf-grenoble.fr (A.B.H.); Pierre.Jean@cesr.fr (P.J.); srazzaque@ssd5.nrl.navy.mil (S.R.); Kent.Wood@nrl.navy.mil (K.S.W.)

Supporting Online Material (SOM)

Materials and Methods: *Fermi*-LAT Data Analysis

The analysis of the LAT data was performed using the *Fermi* Science Tools v9r15 package available from the *Fermi* Science Support Center (FSSC)[1]. The standard onboard filtering, event reconstruction, and classification were applied to the data (*S1*), and the high-quality ("Pass 6 diffuse") event class is used. Throughout the analysis, the "Pass 6 v3 Diffuse" (P6_V3_DIFFUSE) instrument response functions (IRFs) are applied.

Events in the range 0.1–100 GeV were extracted from a $10^\circ \times 10^\circ$ square region of interest (ROI) centered on the known location of V407 Cyg. To greatly reduce contamination from the Earth albedo photons, we excluded time periods when the 10° region around V407 Cyg was observed at a zenith angle greater than 105° and for observatory rocking angles of greater than 52° for observations after mission elapsed time (MET) 273628805 (rocking angles of greater than 43° are excluded for observations prior to this time).

The `gtlike` likelihood fitting tool was used throughout to perform a binned spectral analysis, wherein a spectral-spatial model containing point and diffuse sources is created and the parameters obtained from a simultaneous maximum likelihood fit to the data. The model was constructed by including the 5 brightest point sources from the 1FGL catalog (*S2*) within 15° of the center of the ROI: 1FGL J2021.0+3651, 1FGL J2021.5+4026, 1FGL J2032.2+4127, 1FGL J2030.0+3641, and 1FGL J2111.3+4607. The other 1FGL sources within the ROI were not considered as they are intrinsically faint and not detectable on the timescales of this outburst. The standard models for the Galactic diffuse emission ($gll\_iem\_v02.fit$) and isotropic backgrounds[2] currently recommended by the LAT team were also incorporated into the model. The first three 1FGL sources listed above are known pulsars and were modeled by an exponen-

[1] See the FSSC website for details of the Science Tools: http://fermi.gsfc.nasa.gov/ssc/data/analysis/

[2] Descriptions of the models are available from the FSSC: http://fermi.gsfc.nasa.gov/

tially cut off power-law, while the remaining two sources were modeled by a single power-law with parameters initially set to the values obtained in the 1FGL catalog (*S2*). In the fitting, the Galactic diffuse emission model was scaled by a single power-law with free normalization and index in order to allow for small spectral errors in the model of diffuse emission. All source parameters were left free when investigating the average spectral behavior over the duration of the entire outburst. The parameters of the background point sources were then fixed to their average values when performing likelihood analysis on shorter timescales.

The average spectral behavior

A detailed re-analysis of the LAT data on the reported peak flare days (13 and 14 March) (*S3*) confirms a new γ-ray source not previously reported by the LAT. Fitting the source with a single power-law spectrum yields a flux (>100 MeV) = $(1.3\pm0.2)\times10^{-6}$ photons cm^{-2} s^{-1}, and slope, $\Gamma = 2.2 \pm 0.1$, with a test statistic (TS, (*S4*)) of 111, where the source significance, $\sim \sqrt{TS}$ = 10.5σ. Subsequent analysis indicated that the source was still detectable on timescales of a day through 25 March. Consequently, to investigate the average spectrum and maximize the statistical significance of the detection, we define a time window extended back to the approximate onset of the optical outburst seen in V407 Cyg (10 March 18:00). To include any late low-level emission which would not be detectable on an individual daily basis, the window was extended out to 29 March 00:00. This gives a MET range of 289936803–291513602 and the results of using this defined "active period" are described below.

Using the `gtfindsrc` tool on this active period gives an improved localization over the initially reported one (*12*) at (J2000.0) R.A. = 315.551°, Dec. = 45.737° ($l = 86.958°$, $b = -0.513°$) with a 95% error radius of 0.062°. This γ-ray position is 0.040° offset from the optical position of V407 Cyg; throughout the remainder of the analysis the nominal optical position of V407 Cyg is used. The previously discussed model was used with the `gtlike` tool

to identify the average spectral properties of the source during this period. The source was best fit by an exponentially cut off power-law model ($dN/dE \propto E^{-\Gamma} e^{-(E/E_{\rm c})}$). The flux (>100 MeV) obtained is $(4.4 \pm 0.4\,(\text{stat}) \pm 0.2\,(\text{syst})) \times 10^{-7}$ photons cm^{-2} s^{-1}, with a photon index, $\Gamma = 1.5 \pm 0.2\,(\text{stat}) \pm 0.04\,(\text{syst})$, and a cutoff energy, $E_{\rm c} = 2.2 \pm 0.8\,(\text{stat}) \pm 0.2\,(\text{syst})$ GeV; see below for discussion of how the systematic errors are estimated. The source is detected with a TS = 326.9 ($\sim$18.1σ). The cutoff power-law was compared to a single power-law model by a likelihood ratio test. This gives TS = -2Δlog(Likelihood) = 23.6 and indicates that the addition of the exponential cut off improves the fit at the 4.9σ level compared to a single power-law model.

A number of effects are expected to contribute to the systematic errors. Primarily, these are uncertainties in the effective area and energy response of the LAT as well as background contamination. These are currently estimated by using outlier IRFs that bracket the nominal ones in effective area. These are defined by envelopes above and below the P6_V3_DIFFUSE IRFs by linearly connecting differences of (10%, 5%, 2%) at log(E/MeV) of (2, 2.75, 4), respectively.

Calculating the upper limit

Using the $\sim$19 months of all-sky monitoring data prior to the onset of activity from this source described above it is possible to calculate an average flux upper limit for V407 Cyg in this time range. To this end a new source model is constructed which comprises all 38 1FGL point sources (*S2*) within 15° of the center of the ROI and the standard models for the isotropic and Galactic diffuse emissions. All of the 1FGL sources were modeled with single power-law spectra except for those known to be pulsars in which case an exponentially cut off power-law was applied. An additional point source is inserted at the location of V407 Cyg with an exponentially cut off power-law fixed to the average spectral parameters achieved in the fit to its

active period. The normalization of the source is allowed to be free and a maximum likelihood fit performed. Applying the method of (*S5*) the 95% upper limit on the flux (>100 MeV) is calculated to be 6×10^{-9} photons cm^{-2} s^{-1}.

Exploring the evolution of the outburst

To investigate the evolution of the source flux the data were extracted in one-day segments. A likelihood analysis was performed on each of these segments using the optimized background source model and an exponentially cut off power-law spectrum for the source of interest. The spectral model parameters were fixed to the best obtained average values and only the source normalization and the diffuse background sources were allowed to vary. In each segment the source TS, flux (>100 MeV), and 95% flux (>100 MeV) upper limit were calculated (Table S1). This analysis indicated that the first day in which a significant detection for the source was achieved on March 10 and that the source was detected (TS>9) on daily timescales up to and including 25 March. To further explore the onset of detectable γ-ray emission around the date of the optical detection of the nova (10 March), we divided the data into 6-hr bins. This analysis indicated that the γ-ray signal was isolated to the latter half of this day (Table S2).

Search for spectral variability

We split the *Fermi*-LAT observation period into two time segments with roughly equivalent statistical significance (TS value) for the detection of the source: 10 March 18:00 - 14 March 12:00 (a) and 14 March 12:00 – 29 March 00:00 (b). The best fit spectral index and cutoff energy of the power-law with exponential cutoff are $\Gamma = 1.6 \pm 0.2$ and $E_{\rm c} = (3.0 \pm 0.9)$ GeV, for the first segment (a), and $\Gamma = 1.3 \pm 0.3$ and $E_{\rm c} = (1.7 \pm 0.6)$ GeV for the second segment (b) (Fig. S1). The flux (>100 MeV) varies from $(7.2 \pm 3.1) \times 10^{-7}$ photons s^{-1} cm^{-2} to (3.3±0.8) $\times10^{-7}$ photons s^{-1} cm^{-2} between the two periods while the index and cutoff

energy are statistically equal. For comparison, we fitted the total flux of the power law with exponential cutoff with the segment (b) data by keeping the index and cutoff energy fixed to the values obtained with the best fit of segment (a). It resulted in a difference in log(likelihood) of 0.93. This difference corresponds to a significance of 1.4σ which means that we did not detect any spectral variability.

Parameters of the γ-ray Emission Models

We calculate the π^0 production by pp interactions following the prescription of (*S6*). We use cosmic-ray proton spectra of the form, $N_{\rm p} = N_{\rm p,0}\,(W_{\rm p} + m_{\rm p}\,c^2)^{-s_{\rm p}}\,e^{-W_{\rm p}/E_{\rm cp}}$ (proton GeV^{-1}), where $W_{\rm p}$ is the kinetic energy of protons (GeV) and $m_{\rm p}$ the proton mass. We fit the normalization ($N_{\rm p,0}$), spectral index ($s_{\rm p}$), and the cutoff energy ($E_{\rm cp}$), with the *Fermi*-LAT data. The π^0 emissivity was calculated assuming a solar metallicity. We apply a corresponding nuclear enhancement factor of $\epsilon_{\rm M} = 1.84$ to the π^0 emissivity (*S7*).

The resulting best fit spectral model presented in the main text has a spectral index, $s_{\rm p} = 2.15^{+0.45}_{-0.28}$ and $E_{\rm cp} = 32^{+85}_{-8}$ GeV (1σ uncertainties). Fig. S2 shows the confidence region of the spectral index and cutoff energy fit to the *Fermi*-LAT data. Although the uncertainty of the spectral index is large, its best fit value corresponds to the canonical slope of cosmic-ray protons ($s_{\rm p} \sim 2$) in the first-order Fermi acceleration process. Note that a cutoff energy larger than $\sim$100 GeV is not excluded for spectral indices larger than $\sim$2.5 (95$\%$ confidence level).

The observed γ-ray flux in the π^0 model can be reproduced with a total number of cosmic-ray protons, $\int N_{\rm p}\,dW_{\rm p}$ = $2.0^{+1.1}_{-0.7} \times 10^{45}\,(n_{\rm H}/4 \times 10^8\ {\rm cm}^{-3})^{-1}\,(D/2.7\,{\rm kpc})^2$ in a steady state. The total energy in protons is $\int W_{\rm p}\,N_{\rm p}\,dW_{\rm p}$ = $6.9^{+3.6}_{-2.3} \times 10^{42}\,(n_{\rm H}/4 \times 10^8\ {\rm cm}^{-3})^{-1}\,(D/2.7\,{\rm kpc})^2$ ergs. Here, $n_{\rm H} \approx 4\,n(R)$, is the density of target particles in hydrogen gas in the shock region and $D = 2.7$ kpc is the adopted distance to V407 Cyg (*S8*).

The inverse Compton and bremsstrahlung emissions in the leptonic model are calculated

using the method presented in (*S9*). In our steady state calculation, cosmic-ray electrons in the nova shell interact with infrared photons from the red giant (RG; modeled as a black-body with a temperature of 2500 K and a radius of 500 $R_\odot$) at a distance of $\sim 10^{14}$ cm from the RG. At this distance, the target ion density for the bremsstrahlung process is $n_{\rm H} \approx 4 \times 10^8$ cm^{-3} as in the π^0 model. We use cosmic-ray electron spectra of the form, $N_{\rm e} = N_{\rm e,0}\, W_{\rm e}^{-s_{\rm e}}\, e^{-W_{\rm e}/E_{\rm ce}}$ (electron GeV^{-1}), where $W_{\rm e}$ is the kinetic energy of electrons (GeV). The normalization factor ($N_{\rm e,0}$), spectral index ($s_{\rm e}$), and cutoff energy ($E_{\rm ce}$) are varied to fit the *Fermi*-LAT data.

The resulting best fit leptonic spectral model presented in the main text (Fig. 3) has a spectral index, $s_{\rm e} = -1.75^{+2.40}_{-0.59}$ and $E_{\rm ce} = 3.2^{+2.6}_{-0.1}$ GeV (1σ uncertainties) (Fig. S3). Fig. S4 shows the confidence region of the spectral index and cutoff energy fit to the *Fermi*-LAT data. It presents two optimal zones (confidence level 68%), around $s_{\rm e} = -1.75$ and $s_{\rm e} = 0.25$. The best fit electron level leads to a total number of cosmic-ray electrons in a steady state of $\int N_{\rm e}\, dW_{\rm e}$ = $0.39^{+24.6}_{-0.31} \times 10^{43}\, (D/2.7\,{\rm kpc})^2$ and the total energy in electrons of $\int W_{\rm e}\, N_{\rm e}\, dW_{\rm e}$ = $0.54^{+34.2}_{-0.43} \times 10^{41}\, (D/2.7\,{\rm kpc})^2$ ergs. Note that the uncertainty in the electron spectral index is rather large, and the canonical slope ($s_{\rm e} \sim 2$) expected to arise from the first-order Fermi acceleration process cannot be excluded (99% confidence level).

The difference in the log(likelihood) value for the best fit leptonic model and that of the best fit π^0 model is $\sim$0.05. This difference corresponds to a significance of $\sim 0.3\sigma$ and neither model is statistically preferred over the other.

Optical and Infrared Photometry of V407 Cyg

The optical nova of V407 Cyg was discovered by Nishiyama and Kabashima (*S10*) using an unfiltered CCD image obtained on 10.797 March 2010 UT at the Miyaki Argenteus Observatory in Japan with a 105-mm f/4.0 lens telescope. The pre-outburst image from 7.859 March shows the source 2.5 magnitudes fainter. There are uncertainties in the actual epoch of the nova due to

the three-day gap in the observations. Previous images obtained with the same equipment dating back to April 2008 (Fig. S5) show slow light variations with the total amplitude $\sim$3 mag, which may be attributed to a combination of the Mira-type pulsations of the red giant and activity of the white dwarf.

The bright outburst triggered follow-up photometric observations with a range of instruments and the observations shown in the main paper are summarized here (see Table S3). Many CCD measurements were contributed by enthusiasts from the American Association of the Variable Star Observers (AAVSO), and those who contributed V and $R_{\rm C}$ band CCD photometry presented here were: G. Belcheva (Bulgaria), S. Dvorak, M. Halderman, G. Sjoberg, D. Trowbridge (USA), T. Kantola, M. Luostarinen, A. Oksanen, J. Virtanen (Finland), D. Lane (Canada), S. O'Connor (Bermuda), S. Padovan (Spain), and A. Smirnov (Russia). Observations from the Kwasan Observatory and KANATA telescope are also reported. Small systematic discrepancies between CCD measurements obtained with different telescopes (resulting from different choices of comparison stars and mismatches between instrumental and standard bandpass) were compensated when necessary by using the well sampled AAVSO Bright Star Monitor (BSM) light curve as the primary data set. The BSM photometry used an ensemble of comparison stars in the 8–9 mag range calibrated using the Landolt standards (*S11*).

Fig. S5 shows the combined optical light curve in V and $R_{\rm C}$ bands and the unfiltered CCD measurements by K. Nishiyama and F. Kabashima. A subset of these data are shown in the main paper. The magnitude zero point for the unfiltered measurements was calculated assuming $R_{\rm C} = 6.571$ for the comparison star HIP 103871 as indicated by the BSM photometry, resulting in the peak magnitude $\sim$0.5 mag brighter than the value reported in the discovery (*S10*). The V-band light curve peak of 7.8 mag on 11 March 2010 20:28 communicates a larger brightening, in comparison with the (sparsely covered) historical magnitudes of 14–15, than is apparent in the unfiltered photometric data.

V407 Cyg was also observed in the infrared nine and twenty-five days after the nova explosion using the InSb-photometer (*S12*) at the 1.25-m telescope of the Crimean Laboratory (Sternberg Astronomical Institute). The $JHKLM$ band magnitudes observed are typical for this system around maximum of the Mira pulsation cycle (although with slightly bluer colors), indicating that the RG was still dominating in the infrared (*S13*). Assuming the Galactic extinction ($E_{\rm B-V} = 0.57$) adopted in this paper (*S8*), we converted magnitudes to flux densities (*S14*) and fitted the infrared spectra with Planck's law, which gave a RG temperature of 2500 K at both epochs.

Optical Spectroscopic Measurements

The ejecta velocity, $v_{\rm ej} = 3200 \pm 345$ km s^{-1}, quoted in the main paper was taken as the half width zero intensity of the Hα line measured in a spectrum obtained at the Castanet-Tolosan Observatory and made available online by C. Buil[3]. The measurement was done by fitting a 6th order polynomial to the continuum only in the range λ6420–6655Å, and subtracting from the observed spectrum.

Optical spectra of V407 Cyg obtained with the Nordic Optical Telescope (program P40-423) with resolution 2.2 km s^{-1} (resolving power = 67000) showed that the O I] λ6363Å line displayed a narrow emission peak at -54 km s^{-1} (Fig. S6) on 31 March with FWHM = 26 km s^{-1}, as well as strong absorption on Na I $\lambda\lambda$5889, 5895Å (components at -58 and -51 km s^{-1}). Ca I λ4226.7Å shows a single emission component, centered at -55 kms^{-1}, with FWHM of 7 km s^{-1} that is clearly from the stellar wind. The Balmer lines show strong, broad P Cyg profiles centered at -60 km s^{-1}, indicating absorption through the wind of the RG. The permitted and forbidden Fe-peak lines (i.e., Fe II) display narrow components and the strongest permitted lines display P Cyg profiles with absorption component displacements indicating a

[3]http://astrosurf.com/aras/V407Cyg/v407cyg.htm

RG wind velocity, $v_{\rm w} \approx 10$ km s^{-1}.

References and Notes

S1. W. B. Atwood *et al.* (*Fermi*-LAT collaboration), *Astrophys. J.* **697**, 1071 (2009).

S2. A. A. Abdo *et al.* (*Fermi*-LAT collaboration), *Astrophys. J. Supp.* **188**, 405 (2010).

S3. C. C. Cheung *et al.* (*Fermi*-LAT collaboration), *The Astronomer's Telegram* **2487**, 1 (2010).

S4. J. R. Mattox *et al.*, *Astrophys. J.* **461**, 396 (1996).

S5. O. Helene, *Nucl. Instrum. Methods Phys. Res., Sect. A* **300**, 132 (1991).

S6. T. Kamae, N. Karlsson, T. Mizuno, T. Abe, T. Koi, *Astrophys. J.* **647**, 692 (2006).

S7. M. Mori, *Astropart. Phys.* **31**, 341 (2009).

S8. U. Munari, R. Margoni, R. Stagni, *Mon. Not. R. Astron. Soc.* **242**, 653 (1990).

S9. G. R. Blumenthal, R. G. Gould, *Rev. Mod. Phys.* **42**, 237 (1970).

S10. K. Nishiyama, F. Kabashima, IAU Central Bureau for Astronomical Telegrams, reported by H. Maehara, No. 2199 (2010).

S11. A. U. Landolt, *Astron. J.* **104**, 340 (1992).

S12. A. E. Nadjip, V. I. Shenavrin, V. G. Tichonov, *Proc. Shternberg Astron. Inst.* **58**, 119 (1986).

S13. E. A. Kolotilov, V. I. Shenavrin, S. Y. Shugarov, B. F. Yudin, *Astron. Rep.* **47**, 777 (2003).

S14. M. S. Bessell, J. M. Brett, *Publ. Astron. Soc. Pac.* **100**, 1134 (1988).

S15. M. Watanabe *et al.*, *Publ. Astron. Soc. Pac.* **117**, 870 (2005).

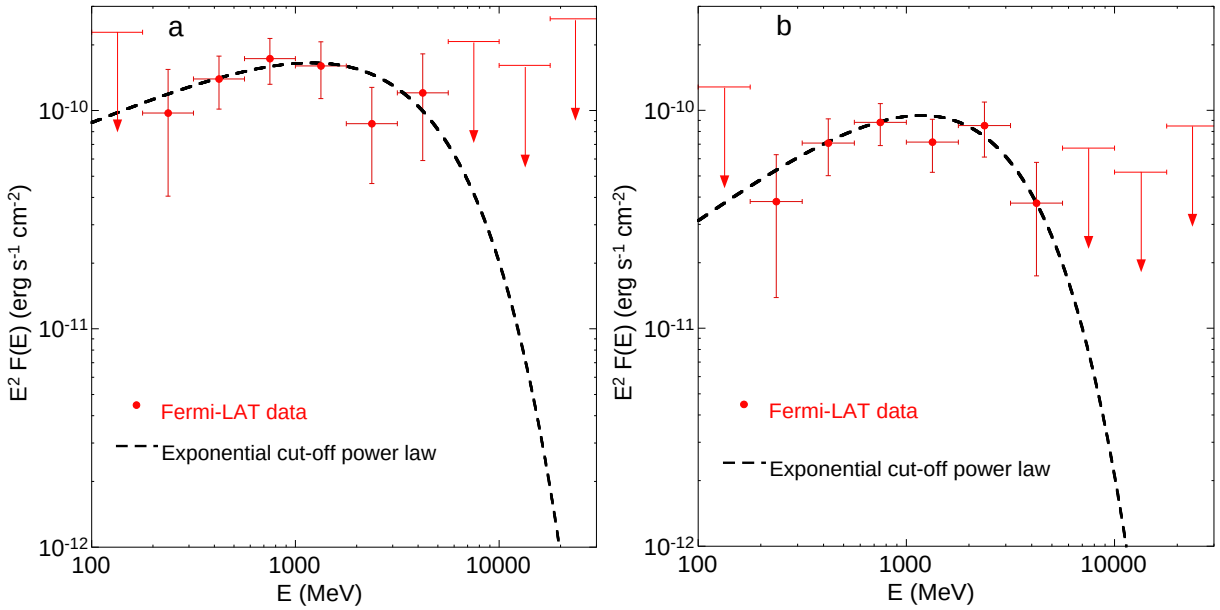

Fig. S1. Spectral energy distribution of V407 Cyg in MeV/GeV γ-rays measured by the *Fermi*-LAT over the period from 10 March 18:00 to 14 March 12:00 (a) and 14 March 12:00 to 29 March 00:00 2010 (b). Horizontal bars indicate energy ranges, vertical bars indicate 1σ statistical errors, and arrows indicate 2σ upper limits. The best fit of a phenomenological power-law with exponential cutoff (dashed line) is presented for the two periods.

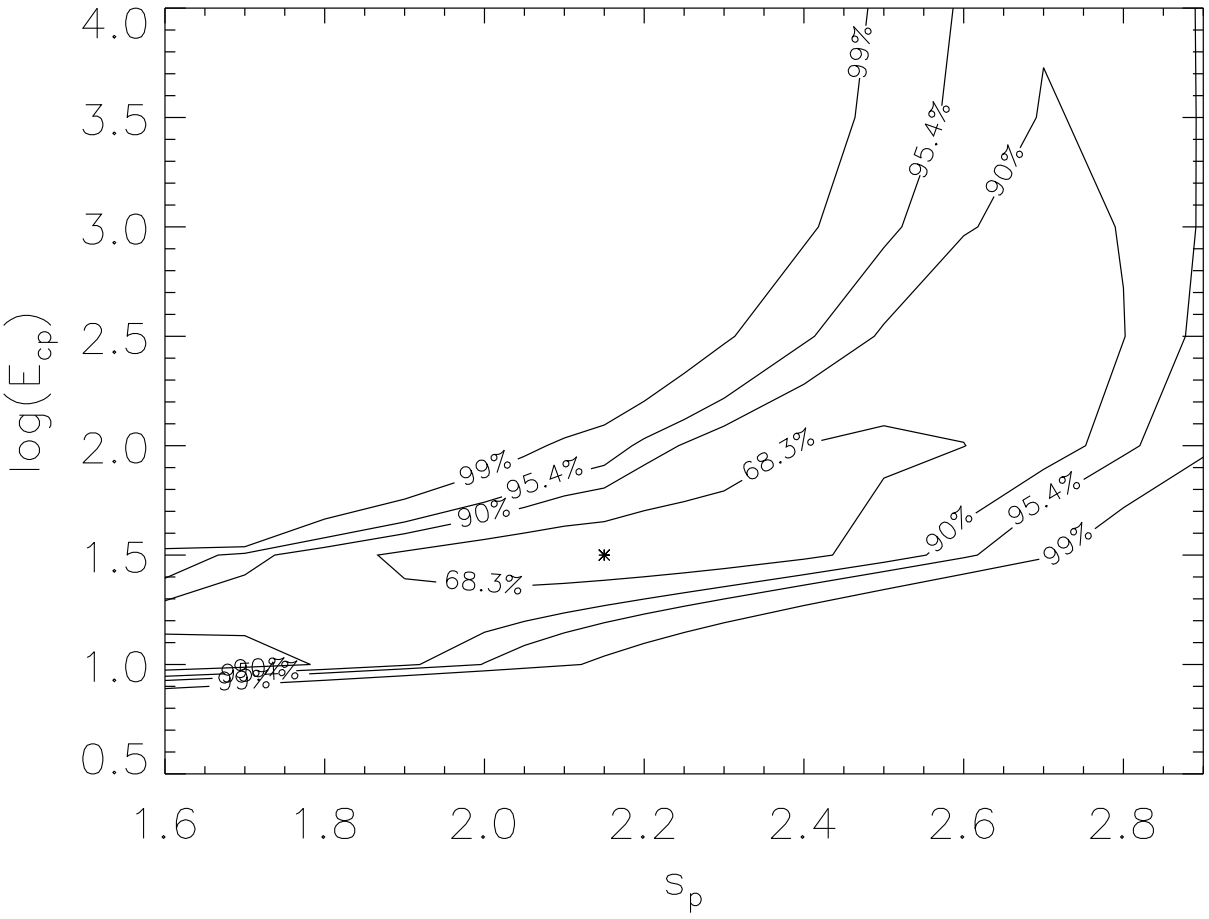

Fig. S2. Confidence region of the spectral slope ($s_{\rm p}$) and logarithm of the cutoff energy ($E_{\rm cp}$ in GeV) fit of the *Fermi*-LAT data for V407 Cyg with the cosmic-ray proton spectrum. The star indicates the best-fit values.

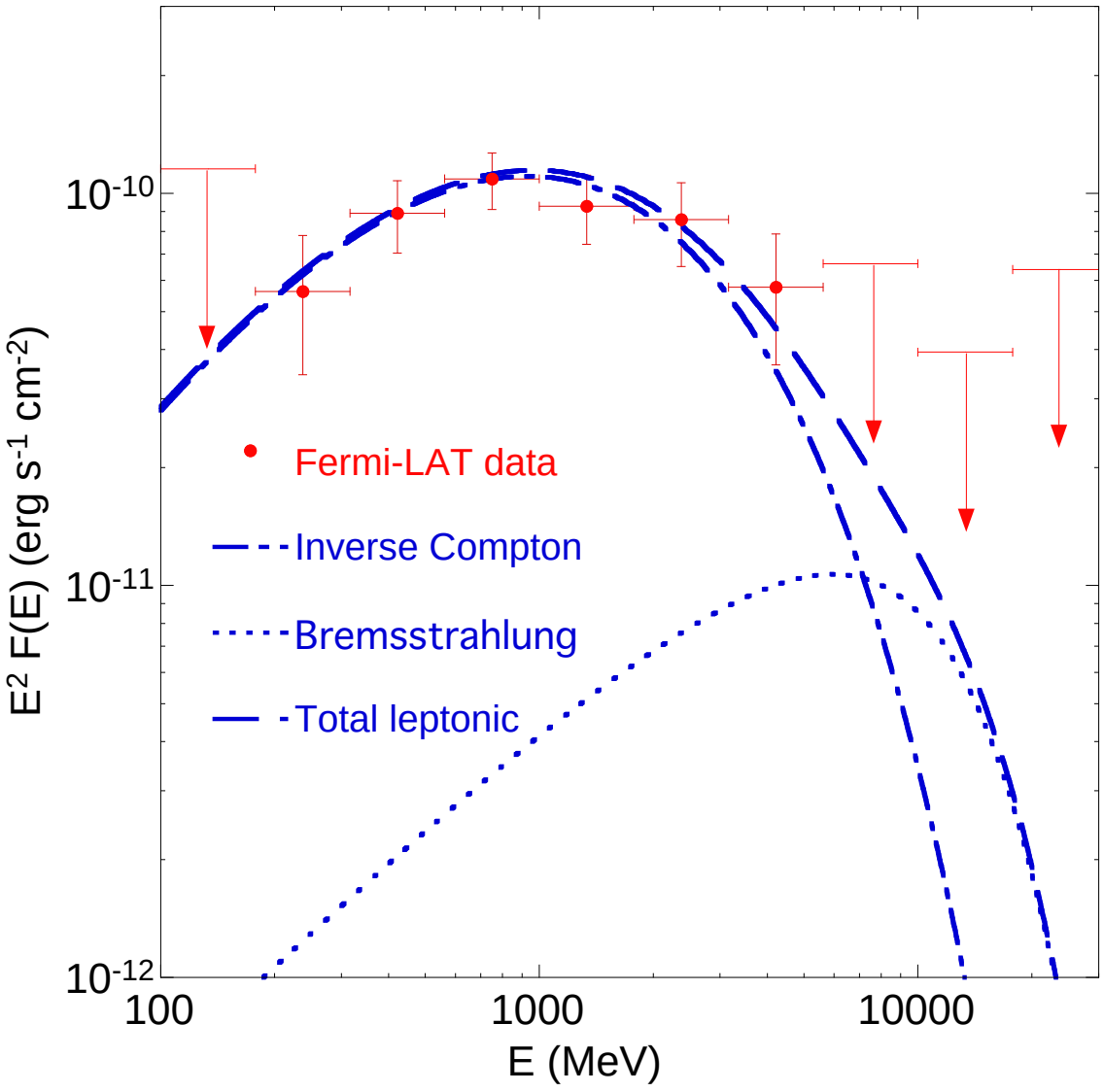

Fig. S3. SED of V407 Cyg in MeV/GeV γ-rays measured by the *Fermi*-LAT over the period 10 March 18:00 – 29 March 00:00 2010. Vertical bars indicate 1σ statistical errors, arrows indicate 2σ upper limits, and horizontal bars indicate energy ranges. The best-fit leptonic model with the separate contributions from the IC (dot-dashed line) and bremsstrahlung (dotted line) spectra indicated, as well as their total (dashed line).

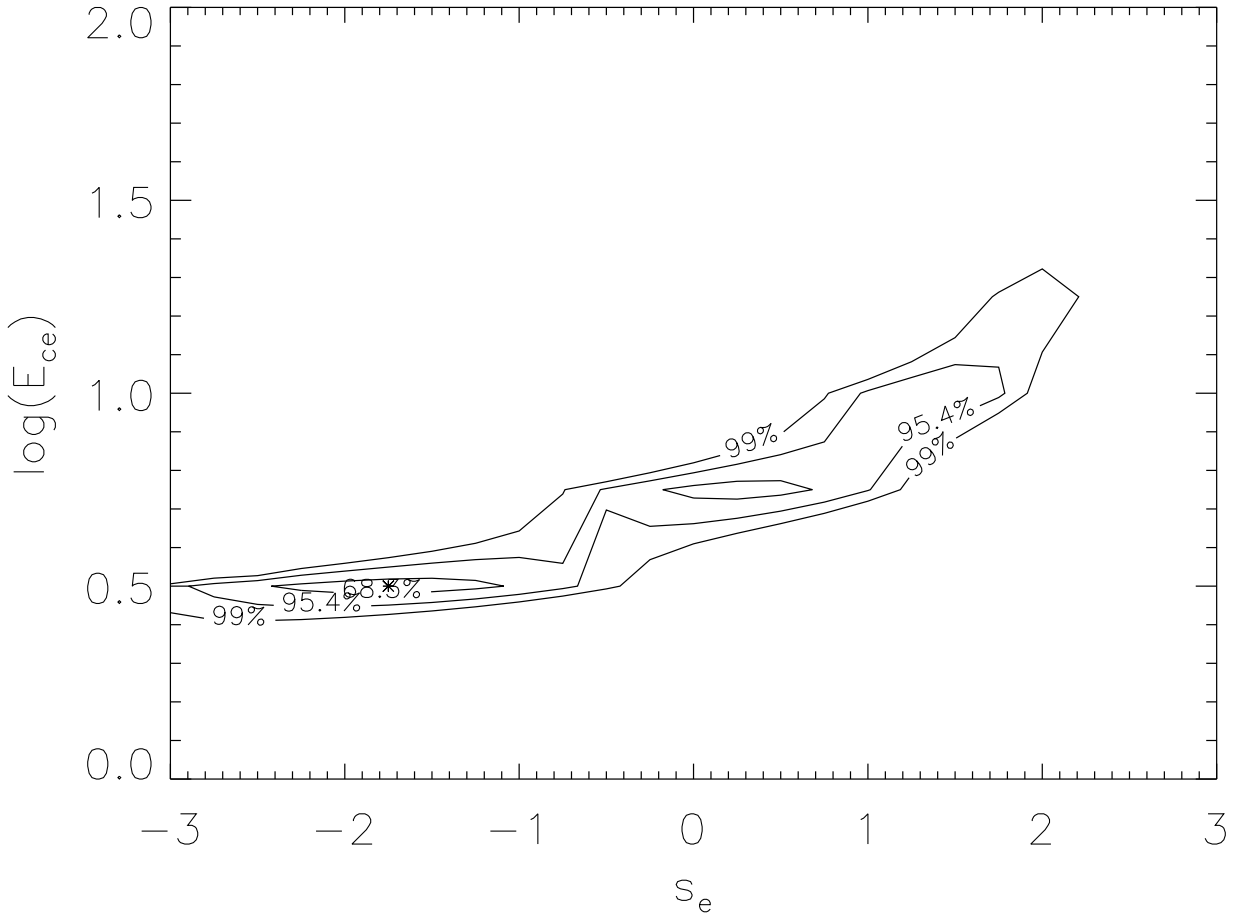

Fig. S4. Confidence region of the spectral slope ($s_{\rm e}$) and logarithm of the cutoff energy ($E_{\rm ce}$ in GeV) fit of the *Fermi*-LAT data for V407 Cyg with the cosmic-ray electron spectrum. The star indicates the best-fit values.

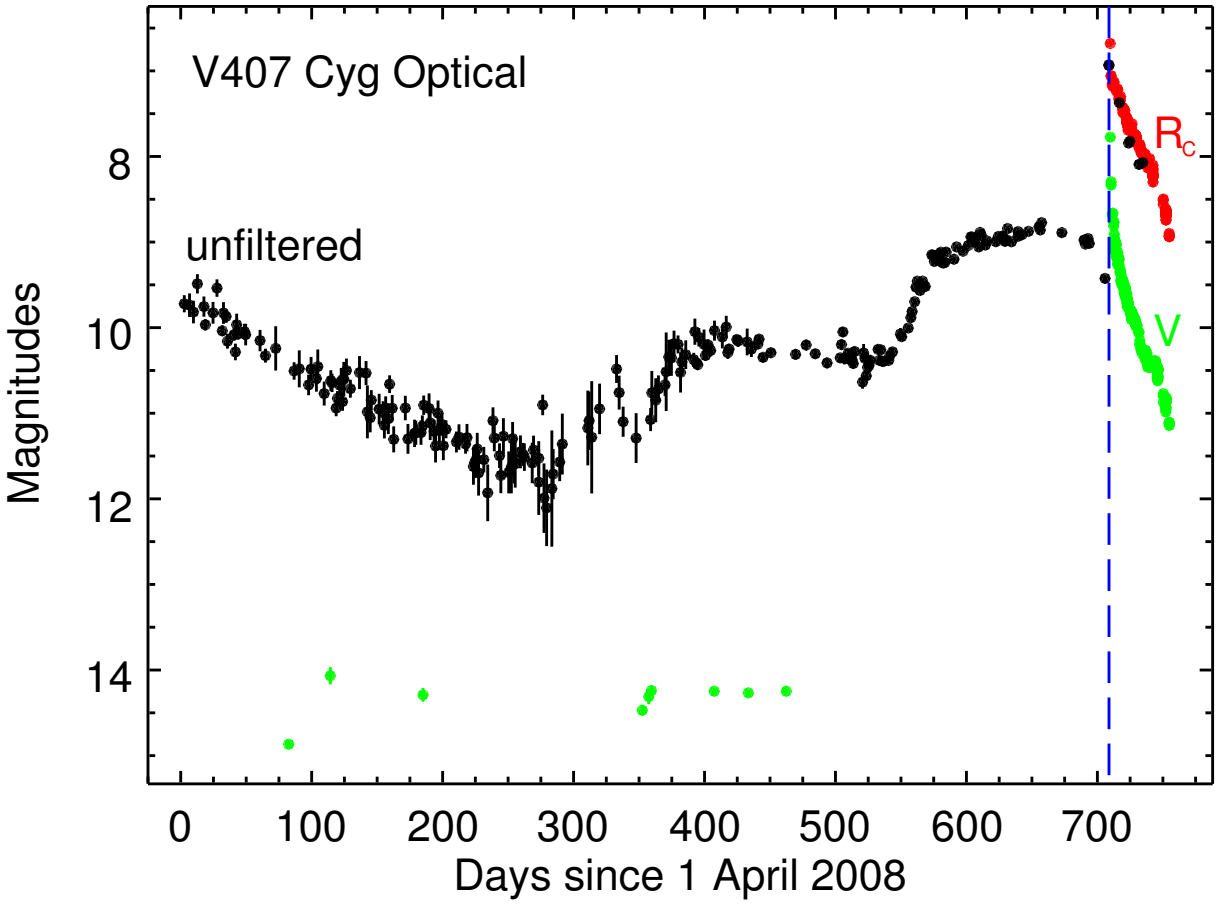

Fig. S5. Optical light curve of V407 Cyg extending back to April 2008. The blue vertical line indicates the epoch of the nova discovery on 10 March 2010.

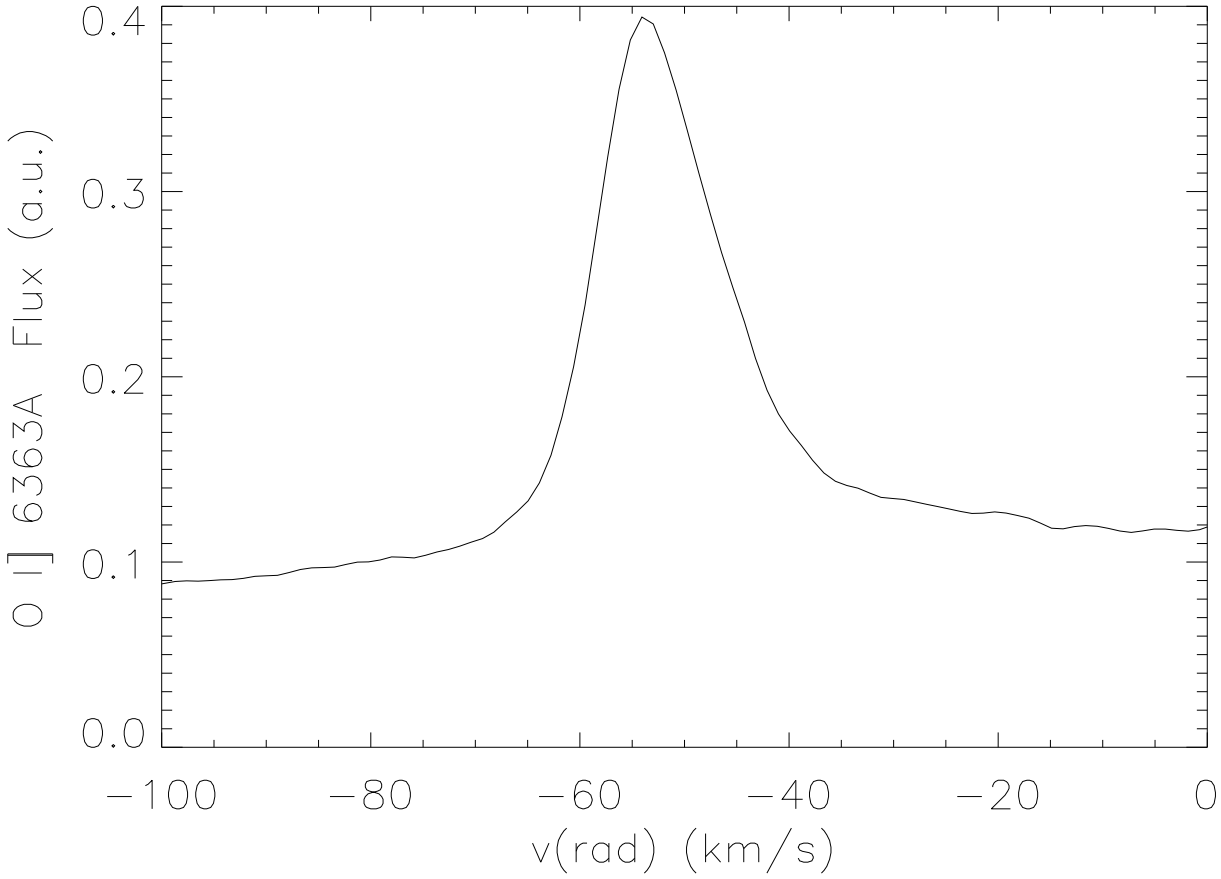

Fig. S6. The O I] λ6303Å line in the heliocentric radial velocity observed in V407 Cyg with the Nordic Optical Telescope on 31 March 2010.

Days since 10 March 2010	TS	Flux (>100 MeV) [10^{-7} photons cm^{-2} s^{-1}]
–4.5	1.5	<4.4
–3.5	0.0	<2.5
–2.5	0.0	<2.2
–1.5	2.2	<3.6
–0.5	0.0	<1.4
0.5	18.9	4.3 ± 1.6
1.5	56.9	7.2 ± 1.7
2.5	12.0	3.7 ± 1.5
3.5	68.4	9.0 ± 1.9
4.5	47.8	8.7 ± 2.0
5.5	27.8	7.3 ± 2.0
6.5	16.7	3.3 ± 1.3
7.5	9.7	3.7 ± 1.8
8.5	11.7	2.7 ± 1.2
9.5	42.2	7.6 ± 2.0
10.5	11.6	2.6 ± 1.2
11.5	15.9	3.7 ± 1.6
12.5	0.5	<2.8
13.5	7.4	<6.9
14.5	19.7	4.9 ± 1.7
15.5	13.3	4.9 ± 1.8
16.5	0.0	<3.5
17.5	4.8	<5.7
18.5	0.0	<1.8
19.5	2.4	<3.5
20.5	0.2	<3.2
21.5	0.9	<3.7
22.5	0.2	<4.2
23.5	0.0	<3.1
24.5	0.0	<2.0
25.5	2.1	<4.3
26.5	0.0	<3.3
27.5	1.9	<3.2
28.5	0.0	<1.8
29.5	0.0	<2.8
30.5	0.2	<3.2
31.5	0.0	<1.7
32.5	0.3	<2.2
33.5	2.1	<4.7
34.5	0.0	<2.2
35.5	3.1	<5.5
36.5	0.0	<1.9
37.5	1.6	<3.5
38.5	0.2	<2.9

Table S1. Daily LAT γ-ray test statistic (TS) and flux values (95% confidence upper limits when TS<9) presented in the main paper. The dates indicated are the centers of the one-day bins.

Time Interval	TS	Flux (>100 MeV) [10^{-7} photons cm^{-2} s^{-1}]
00h-06h	0.0	<3.9
06h-12h	0.0	<6.4
12h-18h	8.0	6.2 ± 3.7
18h-24h	32.0	17.4 ± 5.3

Table S2. Six-hour γ-ray test statistic (TS) and flux values (or 95% confidence upper limits) for 10 March. Note that a flux is reported for the 12h-18h bin despite showing a TS<9 as adopted throughout; the corresponding upper limit was $<15.1\times10^{-7}$ photons cm^{-2} s^{-1}.

Telescope	Filter(s)	Camera
Astrokolkhoz Observatory AAVSO BSM 60-mm, USA	$VR_{\rm C}$	SBIG ST-8XME
Kwasan Observatory 250-mm, Japan	$VR_{\rm C}$	SBIG ST-7XME
Hiroshima University KANATA 1.5-m, Japan	V	TRISPEC (*S15*)
Miyaki Argenteus Observatory 105-mm, Japan	unfiltered	SBIG STL6303E

Table S3. Instruments used for the optical photometric monitoring observations (Fig. S5).